Received 9 October 2024; revised 27 November 2024; accepted 16 December 2024. Date of publication 25 December 2024;
date of current version 8 January 2025.

Digital Object Identifier 10.1109/OJCOMS.2024.3519714

Minimum Operation Altitude for Self-Sustainable Operation of Solar-Powered Fixed-Wing AAVs in Airborne Networks

KHADIJEH ALI MAHMOODI [1] (Member, IEEE), MOHAMMED ELAMASSIE [1] (Senior Member, IEEE), AND MURAT UYSAL [2] (Fellow, IEEE)

[1]Department of Electrical and Electronics Engineering, Ozyegin University, 34794 Istanbul, Türkiye
[2]Engineering Division, New York University Abu Dhabi, Abu Dhabi, UAE

CORRESPONDING AUTHOR: K. ALI MAHMOODI (e-mail: khadijeh.ali@ozu.edu.tr)

ABSTRACT Non-terrestrial networks (NTNs) play a pivotal role in advancing 6G and beyond networks by providing global coverage for backbone infrastructure, wireless access, and backhauling. In particular, fixed-wing autonomous aerial vehicles (AAVs) at tropospheric altitudes are positioned as an efficient platform to provide backhauling for ground-based base stations using high-capacity point-to-point wireless links that operate at either optical or radio spectrum. These AAVs are typically solar-powered to ensure self-sustainability for extended operation durations. Higher altitudes improve energy harvesting by bringing the AAV closer to the Sun and reducing energy consumption due to lower air density. Achieving self-sustainability requires determining the minimum operational altitude at which energy harvested consistently exceeds consumption. In this paper, we derive a closed-form expression for the minimum operational altitude of solar-powered fixed-wing AAVs, ensuring a balance between harvested and consumed energy. Key factors such as geographical location, time of year, AAV mass, and solar panel efficiency are shown to significantly influence this altitude, making them critical to the system's sustainable operation.

INDEX TERMS Non-terrestrial networks, self sustainability, energy harvesting, optimum operation altitude.

I. INTRODUCTION

NON-TERRESTRIAL networks (NTNs) have the potential to provide global coverage and are considered a critical component of 6G and beyond networks [1]. Various forms of space and airborne nodes, such as low earth orbit (LEO) satellites, high-altitude platform stations (HAPSs), and autonomous aerial vehicles (AAVs), can support different network segments, including backbone, wireless access, and backhauling [2]. Fixed-wing AAVs at tropospheric altitudes are an efficient platform for airborne backhauling and use high-capacity point-to-point wireless links to provide backhaul connectivity for ground-based base stations. The required line-of-sight (LoS) transmission for this purpose can be achieved through free-space optical (FSO), microwave or millimeter wave (mmWave) communications [3], [4], [5], [6], [7], [8], [9]. For example, the work in [7] considers an LoS sub-5GHz backhaul link, and discusses the optimal placement of AAV to maximize the total sum rate. The authors in [8] consider a mmWave backhaul system and derive analytical expressions for signal-to-noise ratio (SNR), outage probability, and ergodic capacity. The work in [9] considers a cellular network with a backhaul link and introduces a dynamic resource allocation framework to ensure consistent wireless service for ground users. Similarly, numerous studies have delved into FSO-based airborne backhauling. For example, the work in [3] discusses the potential use cases of FSO-equipped airborne vehicles to address backhaul/fronthaul challenges of wireless networks and presents some simulation results on achievable data rates, scalability, and implementation costs. In [4], the feasibility of airborne FSO communication systems for high-speed train backhauling is analyzed.

Practical deployments often require multiple airborne nodes to establish links between source and destination. To address this, airbone relay-assisted transmission is explored in [5] and [6]. The work in [5] focuses on optimizing AAV

© 2024 The Authors. This work is licensed under a Creative Commons Attribution 4.0 License.
For more information, see https://creativecommons.org/licenses/by/4.0/

placement in FSO relay links to minimize outage probability, thereby enhancing communication efficiency and reducing signal outage risk. In [6], AAV-assisted FSO communication is examined with a focus on dual-hop relay, addressing practical challenges like atmospheric absorption, turbulence, and pointing errors, and their collective impact on system performance.

The seamless integration of LoS backhaul links into existing terrestrial networks is further explored. For example, the work in [10] explores a hybrid FSO/ radio frequency (RF) system and proposes an energy-efficient trajectory optimization scheme for AAVs deployed as relay terminals. They aim to maximize data rates, minimize energy consumption, and optimize energy efficiency, considering cloud movement and other practical constraints. The work in [11] explores a hybrid FSO/RF system with mmWave links from ground to air, and FSO links from air to air and aims to optimize the energy consumption of the fixed wing AAVs as well as the throughput of the system. Additionally, the work in [12] examines a AAV-assisted communication system utilizing hybrid FSO/RF links. It analyzes downlink performance while addressing key challenges such as beam spreading, cloud attenuation, atmospheric turbulence, and AAV misalignment. It also derives several performance metrics, including outage probability, transmission rate, and spectrum efficiency.

Another critical factor in airborne LoS links is energy management and harvesting. Airborne nodes often rely on batteries with limited capacity, but new-generation nodes, in particular fixed-wing AAVs, are powered by solar energy harvested through solar panels installed on their wings [13]. Secondary batteries are charged during daylight to power overnight flights. Therefore, energy constraints must be considered in NTNs. For example, in [14], the authors optimize the three-dimensional (3D) trajectory of a solar-powered fixed-wing AAV, demonstrating adaptability to both LoS and probabilistic channels. In [15], the focus shifts to optimizing trajectories for solar-powered fixed-wing AAVs engaged in communication relay tasks for marine vessels, emphasizing advancements in both transmission quality and energy efficiency. Moreover, [16] formulates a nonconvex trajectory optimization problem for AAV-assisted hybrid FSO/RF links, focusing on maximizing energy efficiency under various operational constraints.

The previous research on the design of energy-efficient flight paths [17] and solar energy harvesting [17], [18], [19] as well as optimized aerodynamic design strategies in mechanical engineering [20], [21] further underscores the importance of altitude management for extending operational time and reducing energy consumption in fixed-wing AAVs. Flying at higher altitudes enhances energy harvesting by positioning the AAV closer to the sun and reduces energy consumption due to lower air density [19]. Therefore, establishing a lower operational altitude is critical to strike a balance between energy efficiency, operational effectiveness, and the varied requirements of missions [22], [23], [24], [25], [26]. For instance, minimizing the distance from take-off to operational duty is critical for time-sensitive missions, enabling prompt response to emergencies [22], [23]. Lower operational altitudes also facilitate more effective remote control capabilities, allowing for rapid intervention if autonomous systems require human supervision [24]. Reduced latency and transmit power requirements (due to shorter transmission distances) are additional factors that favor lower operational altitudes [25]. Certain missions may also require the use of onboard sensors or cameras for data collection, such as environmental monitoring, which necessitates closer proximity to the ground for higher image resolution [26].

From the above discussions, it is clear that operation at lower altitudes bring several advantages. However, it also reduces the levels of harvested energy. To ensure energy sustainability which is a critical issue for HAPS' operation, this work focuses on determining the minimum operational altitude at which energy harvested from solar sources consistently matches the energy consumed throughout the mission. To the best of our knowledge, no previous study has focused on altitude management of airborne backhaul links under energy constraints. Specifically, we consider a solar-powered, fixed-wing AAV operating within the troposphere. We assume that it follows a circular trajectory to provide backhaul for ground-based stations. While different trajectories can be used, a circular trajectory is often preferred in backhauling scenarios as it ensures a constant LoS with the ground station and a stable connection with minimal interruptions. We first present comprehensive energy harvesting models that consider geographical location, day of the year, and time of the day, as well as the efficiency and size of the solar panel and altitude-dependent atmospheric transmittance. Similarly, we present energy consumption models that consider various AAV parameters such as total weight, wing area, velocity, drag coefficient, propeller efficiency, aspect ratio of the wings, and environmental parameters such as air density. Then, we formulate and solve an optimization problem such that the minimum altitude is determined at which the harvested energy of the AAV is equal to the consumed energy during the mission. We further present numerical results to demonstrate the effect of system and environmental parameters on the minimum operation altitude.

The remaining of the paper are structured as follows: In Section II, we present the system model, detailing energy consumption and energy harvesting models. In Section III, we formulate an optimization problem to derive the minimum operational altitude for self-sustainability and provide a closed-form solution. In Section IV, numerical results are presented along with discussions on performance. The paper concludes with Section V.

II. SYSTEM MODEL

We consider a fixed-wing AAV that operates within the troposphere (i.e., up to 10 km altitude) [27]. Trajectories can

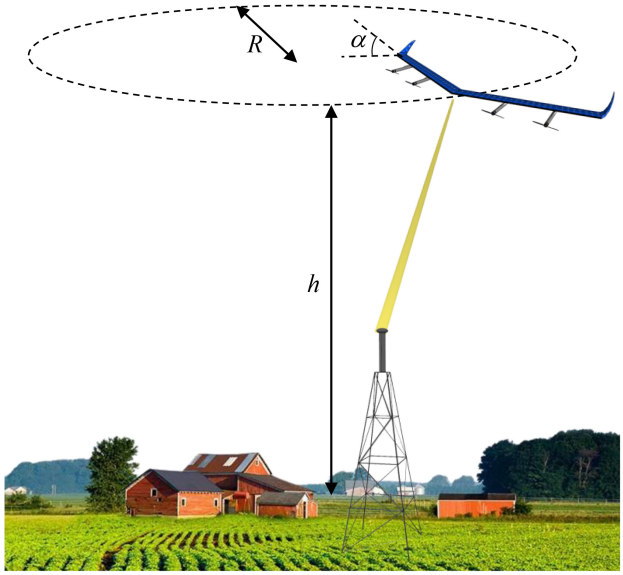

FIGURE 1. Fixed-wing solar powered AAV based communication system.

take different forms including elliptical, straight-line, circular among others. Circular trajectories are advantageous for ensuring a predictable energy consumption during missions like continuous surveillance or communication relay and for maintaining stable LoS communication [3], [7], [18]. In this paper, we assume that the AAV follows a predefined circular trajectory with a constant speed in a given geographical area and provides backhauling for base stations on the ground. The AAV is equipped with solar panels, enabling it to operate for extended durations without the need for frequent battery recharging. For backhauling, it establishes a LoS link with the base station.

A. ENERGY CONSUMPTION MODEL

We assume that the fixed-wing AAV has a constant velocity of v and follows a circular trajectory with a radius R at a bank angle α (See Figure 1). The banking angle defines the angle between the wing in the lateral plane and the horizontal plane and is calculated as $\alpha = \tan^{-1}(v^2/gR)$, where g is the acceleration due to gravity [18].

In circular level flight, the power consumption of a fixed wing AAV consists of two main components [28], namely parasitic power and induced power. Parasitic power refers to the energy lost due to aerodynamic drag and other forms of resistance that occur during flight. This power is necessary to overcome the drag forces acting on the AAV. On the other hand, induced power relates to the energy required to generate lift and sustain the AAV's flight. This power is essential for maintaining altitude and is directly associated with the aerodynamic lift forces. The total power consumption of the fixed wing AAV is given by [28]

$$P_{\text{out}} = \underbrace{\frac{\rho v^3 A_{\text{w}} C_{\text{D}}}{2\eta_{\text{prop}}\cos^2(\alpha)}}_{\text{parasite}} + \underbrace{\frac{2W^2}{\eta_{\text{prop}}\cos^2(\alpha)(\pi e_0 A_{\text{r}})\rho A_{\text{w}} v}}_{\text{induced}}, \quad (1)$$

where A_{w} is the wing area, C_{D} is the drag coefficient, η_{prop} is the propeller efficiency, e_0 is the Oswald efficiency, A_{r} is the aspect ration of the wing, W is the weight of the AAV, defined as $W = mg$, where g represents the acceleration due to gravity, and m represents the mass of the AAV.

In (1), ρ denotes air density which depends on the operation altitude. Assuming dry air[1] and let p_0 and t_0 stand for sea level standard atmospheric pressure and standard temperature, respectively, air density at a given altitude[2] is given by [29]

$$\rho = \frac{p_0 \mu}{\varpi t_0}\left(1 - \frac{\sigma h}{t_0}\right)^{\frac{g\mu}{\varpi\sigma}-1}, \quad (2)$$

Here, μ, ϖ, and σ stand, respectively, for molar mass of dry air, ideal gas constant, and temperature lapse rate.[3]

For a mission with a duration of T hours, the energy consumption is then calculated as

$$E_{\text{out}} = TP_{\text{out}} \quad (3)$$

Replacing (2) in (1) and (1) in (3), we obtain (4), given at the bottom of the page. Eq. (4) can be rewritten in a more compact form as

$$E_{\text{out}} = \Psi(1 + \text{K}h)^{\kappa} + \Phi(1 + \text{K}h)^{-\kappa}, \quad (5)$$

where $\text{K} = -\sigma/t_0$, $\kappa = g\mu/(\varpi\sigma) - 1$, $\Psi = Tp_0\mu v^3 A_{\text{w}} C_{\text{D}}/(2\varpi\iota_0\eta_{\text{prop}}\cos^2(\alpha))$, and $\Phi = 2TW^2\varpi\iota_0/\eta_{\text{prop}}\cos^2(\alpha)(\pi e_0 A_{\text{r}})p_0\mu A_{\text{w}} v$.

B. ENERGY HARVESTING MODEL

Let A_{s} denote the area of the solar panel mounted flat on the AAV's wings with no additional tilt angle relative to the wing surface [30].[4] Let η_{sc} and t_{start} represent the solar

[1]Dry air refers to atmospheric air that does not contain any significant amount of water vapor.

[2]This formula is applicable up to the altitude of $h = 10$ km.

[3]The rate at which atmospheric temperature decreases with an increase in altitude under standard conditions.

[4]Unlike deformable solar-powered AAVs, which adjust their wing angles to optimize solar energy intake by altering the dihedral angle of the outer wings [31], [32], our AAV employs a fixed-wing design with minimal tilt due to mechanical constraints [18].

$$E_{\text{out}} = T\frac{\frac{p_0\mu}{\varpi\iota_0}\left(1 - \frac{\sigma h}{t_0}\right)^{\frac{g\mu}{\varpi\sigma}-1} v^3 A_{\text{w}} C_{\text{D}}}{2\eta_{\text{prop}}\cos^2(\alpha)} + \frac{2W^2}{\eta_{\text{prop}}\cos^2(\alpha)(\pi e_0 A_{\text{r}})\frac{p_0\mu}{\varpi\iota_0}\left(1 - \frac{\sigma h}{t_0}\right)^{\frac{g\mu}{\varpi\sigma}-1} A_{\text{w}} v}. \quad (4)$$

panel's efficiency and the flight's start time, respectively. The total harvested energy (measured in watt-hours) is given by:

$$E_{\text{in}} = \int_{t=t_{\text{start}}}^{t_{\text{start}}+T} \psi A_{\text{s}} \eta_{\text{sc}} G_{\text{in}}(t) dt, \tag{6}$$

where $G_{\text{in}}(t)$ is the instantaneous solar intensity, and ψ is the atmospheric transmittance. The instantaneous solar intensity depends on the time of day and is calculated as (7) [19], given at the bottom of the page. In (7), ξ_{m} is the maximum elevation angle of the Sun, t_s and t_e are, respectively, the start and end times of instantaneous solar intensity. G_{m} is the maximum instantaneous radiation intensity that occurs at t_{max}, which corresponds to the moment when solar irradiance is perpendicular to the AAV's wing. The value of t_{max} is defined as

$$t_{\text{max}} = t_{\text{sunrise}} + (\xi_{\text{m}} - \alpha)\tau/(2\xi_{\text{m}}) \tag{8}$$

where t_{sunrise} is the time of sunrise, α is the bank angle defining the tilt of the wings relative to the horizontal flight plane (as discussed in Section II-A), and τ is the duration of daylight. The start and end times of the instantaneous solar intensity are given as $t_s = t_{\text{sunrise}}$, and $t_e = 2t_{\text{max}} - t_{\text{sunrise}}$, respectively.

Under the assumption of a zero bank angle ($\alpha = 0$),[5] the maximum instantaneous radiation intensity occurs at $t_{\text{max}} = 12$, corresponding to solar noon. In this scenario, the end time of the instantaneous solar intensity, t_e, becomes equal to $t_e = t_{\text{sunset}}$, which is the time when the Sun sets. The sunrise and sunset times are defined as $t_{\text{sunrise}} = 12 - \tau/2$ and $t_{\text{sunset}} = 12 + \tau/2$, respectively. Consequently, (7) simplifies to (9), given at the bottom of the page.

To consider the effect of atmospheric conditions, we use the following atmospheric transmittance formula obtained through the LOWTRAN 7 which is a widely used propagation model [18]. According to this formulation which assumes a standard atmospheric profile for clear to mildly hazy weather, with altitude as the main variable, the atmospheric transmittance is given by [18]

$$\psi = -0.2804 \exp\left(-\frac{h}{3500}\right) + 0.8978. \tag{10}$$

It should be note that this model is most accurate for clear or lightly cloudy skies, with reduced precision in extreme weather or highly variable regions.

By substituting (10) in (6) and solving the resulting integral, we find the harvested energy as

$$E_{\text{in}} = \psi E_{\text{in,U}}, \tag{11}$$

where $E_{\text{in,U}}$ is the harvested energy assuming unity transmittance and is given by (12), given at the bottom of the page. Replacing (12) in (11) we obtain

$$E_{\text{in}} = A_{\text{in}} + B_{\text{in}} \exp(C_{\text{in}} h), \tag{13}$$

where $A_{\text{in}} = 0.8978\, E_{\text{in,U}}$, $B_{\text{in}} = -0.2804\, E_{\text{in,U}}$, and $C_{\text{in}} = -1/3500$.

III. OPTIMIZATION OF MINIMUM OPERATION ALTITUDE

Our primary objective is to identify the minimum altitude at which the AAV can maintain flight solely through harvested solar energy. We define the net energy defined as energy harvested minus energy consumption, i.e., $E_{\text{net}} = E_{\text{in}} - E_{\text{out}}$. Accordingly, we define the optimization problem accordingly as

$$\begin{aligned} &\min \ \ h \\ &\text{s.t.} \ \ E_{\text{net}} = 0. \end{aligned} \tag{14}$$

To find the altitude where the net energy balance is zero, we need to satisfy

$$E_{\text{in}} = E_{\text{out}}. \tag{15}$$

By Replacing (5) and (13) within (15), we can write

$$\begin{aligned} A_{\text{in}} + B_{\text{in}} \exp(C_{\text{in}} h_{\text{min}}) = \Psi(1 + \text{K}h_{\text{min}})^{\kappa} \\ + \Phi(1 + \text{K}h_{\text{min}})^{-\kappa}. \end{aligned} \tag{16}$$

First, note that the right-hand side of (16) contains two terms in the form $(1 + \text{K}h_{\text{min}})^n, n \in \{\kappa, -\kappa\}$. Here, $\text{K} = -\sigma/t_0$ yields extremely small values for practical values of the sea-level standard temperature (t_0) and the temperature

[5] In typical AAV operations on a circular track, the AAV's velocity is in the range of several meters per second, while the radius of its circular path spans several kilometers. This results in a negligible bank angle, i.e., $\alpha \ll 1^\circ$ which can be efficiently ignored.

$$G_{\text{in}}(t) = \begin{cases} G_{\text{m}} \sin\left(\frac{2\xi_{\text{m}}}{t_{\text{s}} - t_{\text{e}}}(t - t_{\text{s}})\right), & t_{\text{s}} < t < t_{\text{max}} \\ G_{\text{m}} \sin\left(\left(2\xi_{\text{m}} - \frac{2\xi_{\text{m}}}{t_{\text{s}} - t_{\text{e}}}(t - t_{\text{e}})\right)\right), & t_{\text{max}} < t < t_{\text{e}} \end{cases}, \tag{7}$$

$$G_{\text{in}}(t) = \begin{cases} G_{\text{m}} \sin\left(\frac{2\xi_{\text{m}}}{\tau}(t - t_{\text{sunrise}})\right), & t_{\text{sunrise}} < t < 12 \\ G_{\text{m}} \sin\left(\left(2\xi_{\text{m}} - \frac{2\xi_{\text{m}}}{\tau}(t - t_{\text{sunset}})\right)\right), & 12 < t < t_{\text{sunset}} \end{cases}, \tag{9}$$

$$\begin{aligned} E_{\text{in,U}} = \frac{180\tau A_{\text{s}} \eta_{\text{sc}} G_{\text{m}}}{\xi_{\text{m}} \pi} \\ \times \left[\cos\left(\frac{2\xi_{\text{m}}}{\tau}(12 - t_{\text{sunset}})\right)\left(\cos\left(\frac{\xi_{\text{m}}}{\tau}T\right) - 1\right) + \sin\left(\frac{2\xi_{\text{m}}}{\tau}(12 - t_{\text{sunrise}})\right)\sin\left(\frac{\xi_{\text{m}}}{\tau}T\right)\right]. \end{aligned} \tag{12}$$

lapse rate (σ). For example, assuming $t_0 = 288.15^{\circ}$ K and $\sigma = 0.0065^{\circ}$ K/m, we get $\mathrm{K} = 0.000022\mathrm{m}^{-1}$. Additionally, the maximum altitude of a fixed-wing AAV is limited to a few kms. Therefore, the product of K and $h_{\min}$ (i.e., $\mathrm{K}h_{\min}$) remains very small and satisfies $\mathrm{K}h_{\min} \ll 1$. As a result, we can use the approximation $(1+x)^n \approx 1 + nx$ for $x \ll 1$, and write $(1+\mathrm{K}h_{\min})^n \approx 1 + n\mathrm{K}h_{\min}$. Utilizing this approximation, (16) can be written as

$$A_{\text{in}} + B_{\text{in}} \exp(C_{\text{in}} h_{\min}) = (\Psi - \Phi)\kappa \mathrm{K} h_{\min} + (\Psi + \Phi), \quad (17)$$

Let $A_F = (\Psi + \Phi - A_{\text{in}})/B_{\text{in}}$ and $B_F = (\Psi - \Phi)\kappa \mathrm{K}/B_{\text{in}}$, we can re-arrange (17) as

$$\exp(C_{\text{in}} h_{\min}) \approx B_F h_{\min} + A_F, \quad (18)$$

If we exponentiate both side of (18) and then raise both side of the resultant expression to the power of $-C_{\text{in}}/B_F$, we can write

$$\begin{aligned} &\exp\left(-\frac{C_{\text{in}}}{B_F}\exp(C_{\text{in}} h_{\min})\right) \\ &\approx \exp\left(-\frac{C_{\text{in}}}{B_F}A_F\right)\exp(-C_{\text{in}} h_{\min}), \end{aligned} \quad (19)$$

If we multiply both sides of (19) by $-C_{\text{in}}/B_F \exp(C_{\text{in}} h_{\min})$, we can rearrange it as

$$\begin{aligned} &\frac{-C_{\text{in}}}{B_F}\exp(C_{\text{in}} h_{\min})\exp\left(-\frac{C_{\text{in}}}{B_F}\exp(C_{\text{in}} h_{\min})\right) \\ &\approx \frac{-C_{\text{in}}}{B_F}\exp\left(-\frac{C_{\text{in}}}{B_F}A_F\right). \end{aligned} \quad (20)$$

It can be observed that (20) is in the form of $xe^x = y$. Utilizing Lambert-W function, we can solve (20) for $h_{\min}$ as

$$h_{\min} \approx \frac{1}{C_{\text{in}}}\ln\left(-\frac{B_F}{C_{\text{in}}}\mathrm{W}\left[\frac{-C_{\text{in}}}{B_F}\exp\left(-\frac{C_{\text{in}}}{B_F}A_F\right)\right]\right). \quad (21)$$

Now, if we substitute $A_F = (\Psi + \Phi - A_{\text{in}})/B_{\text{in}}$, $B_F = (\Psi - \Phi)\kappa \mathrm{K}/B_{\text{in}}$ in (21), the final form of the minimum altitude can be written as (22), given at the bottom of this page.

IV. NUMERICAL RESULTS

In this section, based on the derived expression in (22), which assumes $\alpha = 0$ for the calculations of the energy harvesting,[6] we present numerical results to demonstrate the effect of system and environmental parameters on the minimum operation altitude. Specifically, we consider a fixed-wing AAV with a wing area of $A_{\text{w}} = 20\ \mathrm{m}^2$ and a total mass of $m = 50$ kg, following a circular trajectory with a radius of $R = 16$ km at a velocity of $v = 25$ m/s. Additional simulation parameters are provided in Section IV.

[6]It can be noted that, for the given parameters under consideration, the bank angle is not zero and is equal to 0.228. However, for such a small bank angle, the level of harvested energy remains approximately the same.

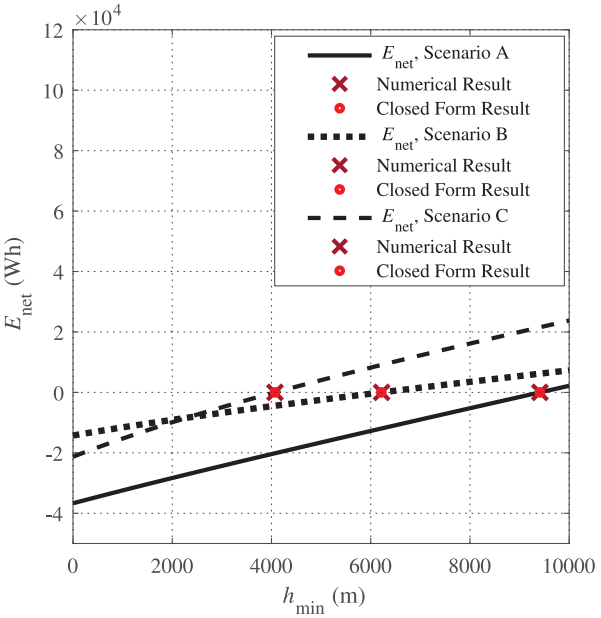

FIGURE 2. Net energy levels versus altitude under various scenario conditions.

We consider three climate types including midlatitude climate type with the latitude of $L = 40°$, tropical climate type with the latitude of $L = 7°$, and subarctic climate type with the latitude of $L = 65°$. We assume four representative days of the year in various seasons including spring ($d = 100^{\text{th}}$ day of the year), summer ($d = 173^{\text{rd}}$ day of the year), fall $d = 240^{\text{th}}$ day of the year), and winter ($d = 340^{\text{th}}$ day of the year).

To verify the accuracy of the approximate derived expression in (22) for the minimum operation altitude, we first compare it with the numerically computed optimal value as shown in Figure 2. For this numerical computation, we consider the expression in (16) and vary the altitude from $h = 0$ km to $h = 10$ km. We identify the point at which the net energy E_{net} equals zero. As examples, we analyze three scenarios with the following parameters:

- Scenario A: $d = 100$, $L = 40°$, $m = 50$ kg, $v = 25$ m/s, $\eta_{\text{sc}} = 0.4$.
- Scenario B: $d = 240$, $L = 65°$, $m = 40$ kg, $v = 20$ m/s, $\eta_{\text{sc}} = 0.2$.
- Scenario C: $d = 173$, $L = 40°$, $m = 60$ kg, $v = 30$ m/s, $\eta_{\text{sc}} = 0.3$.

The solid, dashed, and dotted black lines represent the numerical values of net energy considering scenario A, B, and C, respectively. In Figure 2, the red cross signs denote the numerically computed optimal altitude. Conversely, the

$$h_{\min} \approx \frac{1}{C_{\text{in}}}\ln\left(-\frac{(\Psi - \Phi)\kappa \mathrm{K}}{C_{\text{in}} B_{\text{in}}}\mathrm{W}\left[-\frac{C_{\text{in}} B_{\text{in}}}{(\Psi - \Phi)\kappa \mathrm{K}}\exp\left(-\frac{C_{\text{in}}(\Psi + \Phi - A_{\text{in}})}{B_F B_{\text{in}}}\right)\right]\right). \quad (22)$$

TABLE 1. System parameters.

Parameter	Variable	Value
Wing Area	A_{w} (m^2)	20 [33]
Total Mass	m (kg)	50 [33]
Drag Coefficient	C_{D}	0.007 [19]
Propeller Efficiency	η_{prop} (%)	80
Aspect Ratio of the Wing	A_{r}	6 [6]
Circle of Radius	R (km)	16
Acceleration	g $(\mathrm{m/s}^2)$	9.8
Solar Panel Efficiency	η_{sc} (%)	37.5 [19]
Ideal Gas Constant	ϖ (J/mol.K)	8.3144
Molar Mass of Dry Air	μ (kg/mol)	0.0289
Oswald Efficiency	e_0	0.7
Sea Level Standard Atmospheric Pressure	p_0 $(\mathrm{J/m}^3)$	101325
Sea Level Standard Temperature	t_0 (K)	288.15
Attached Solar Panel Area	$\mathrm{A_w}$ (m^2)	20
Solar Constant	G_{sc} $(\mathrm{W/m}^2)$	1366.1
Temperature Lapse Rate	σ (K/m)	0.0069
UAV's Velocity	v (m/s)	25 [34]
Latitude	L	40°, 7°, 65°
Axial Tilt	ε	23.44°
Operation Altitude Range	h (km)	0-10 [33]
Mission Duration	T (hours)	24

red circles indicate the optimal altitude obtained from the closed-form expression in (22).

For Scenarios A, B and C, the exact optimal altitudes are found to be $h = 9.41$ km, $h = 6.22$ km, and $h = 4.07$ km, based on the numerical computation. The derived closed-form expression in (22) yield $h_{\min} = 9.4084$ km, $h_{\min} = 6.2146$ km, and $h_{\min} = 4.06$ km. The close alignment between these demonstrate the accuracy of the derived approximate expression. Specifically, the differences between the actual numerical optimal altitudes and the values obtained from (22) are minimal, with discrepancies of only 0.0016 km (or 1.6 meters) for the Scenario A, 0.0054 km (or 5.4 meters) for the Scenario B, and 0.01 km (or 10 meters) for the Scenario C.

From this figure, we can further observe how the altitude optimization helps with energy sustainability. For example, in Scenario A, consider an arbitrarily selected operation altitude of $h = 4$km instead of the optimal altitude. This gives the net energy $E_{\mathrm{net}} = -20\,\mathrm{kWh}$ over a 24-hour operation indicating that an additional 20 kWh is required to sustain the flight for the full duration. However, at the optimized altitude of $h = 9.4\,\mathrm{km}$, the net energy becomes $E_{\mathrm{net}} = 0\,\mathrm{kWh}$ ensuring that the AAV achieves energy sustainability over the entire 24-hour period. Beyond this altitude, the net energy remains positive, meaning the AAV can fully rely on the harvested solar energy throughout the operation.

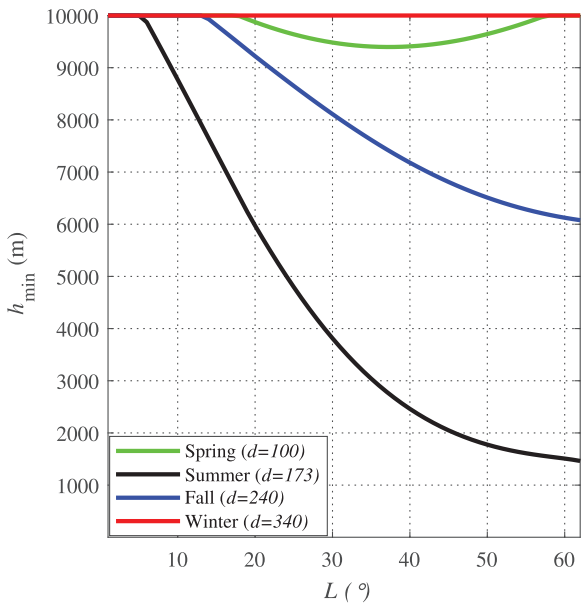

FIGURE 3. Minimum altitude with respect to latitude.

After we verify the accuracy of the derived expression, we now use (22) to investigate the effect of various parameters. Figure 3 illustrates the variation in minimum altitude versus different latitudes spanning from tropical to

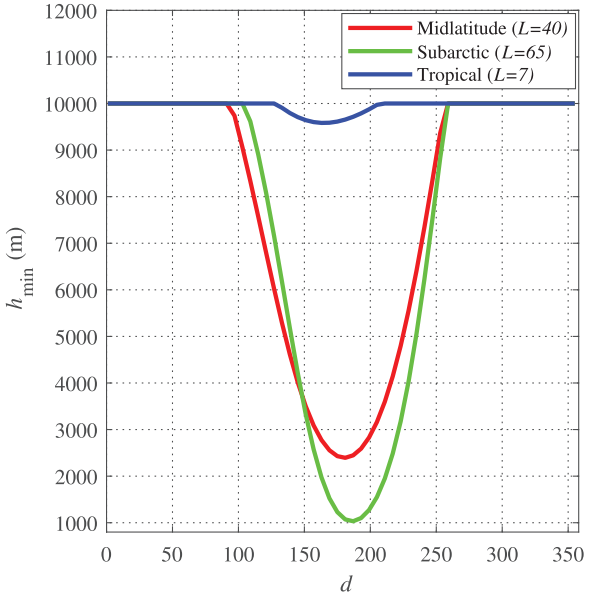

FIGURE 4. Minimum altitude with respect to day.

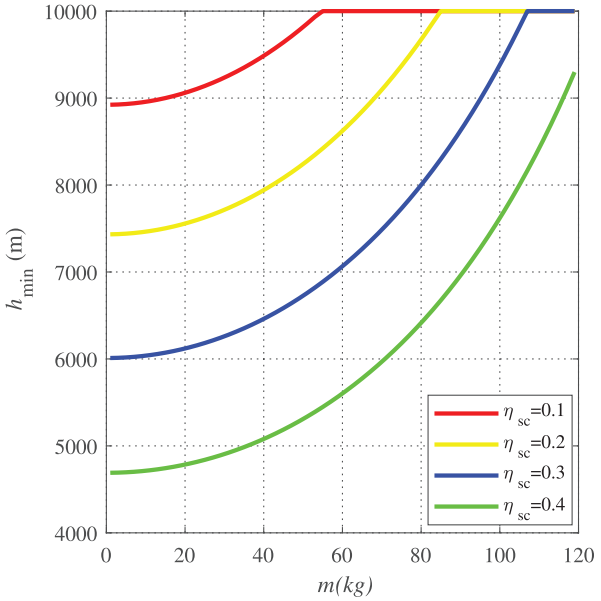

FIGURE 5. Minimum altitude with respect to mass of the AAV.

subarctic climates. Representative days of the year from spring to winter are considered. For example, consider $L = 40°$, i.e., midlatitude climate type, the minimum altitude reaches its minimum in summer and gradually increases through fall and winter. For the location associated with $L = 40°$, the minimum altitude is $h_{\min} = 9.4\,\text{km}$, $h_{\min} = 2.46\,\text{km}$, $h_{\min} = 7.1\,\text{km}$, and $h_{\min} = 10\,\text{km}$, respectively, in spring, summer, fall, and winter. In winter time, this value remains consistent across all latitudes. In the spring season, the minimum altitude initially decreases with increasing latitude until a certain point in subarctic regions ($L < 38°$), after which it begins to rise. In fall and summer, the minimum altitude continually decreases with increasing the latitude. A lower minimum altitude signifies that the fixed-wing AAV can harvest more solar energy, requiring less altitude to meet the constraint specified in (14), ensuring energy harvesting equals energy consumption over the mission duration.

Figure 4 depicts the variation in minimum altitude versus different days throughout the year. Midlatitude, subarctic, and tropical climates are considered. For a specific latitude, the minimum altitude required for sustainable AAV operation initially decreases with the progression of days until a specific point on $d = 180^{\text{th}}$, at which it begins to ascend. A lower minimum altitude indicates that the fixed-wing AAV can efficiently harvest more solar energy, necessitating less altitude to fulfill the constraint specified in (14). For example, on $d = 180^{\text{th}}$ day of the year, the minimum altitudes are $h_{\min} = 1\,\text{km}$, $h_{\min} = 2.4\,\text{km}$, and $h_{\min} = 9.5\,\text{km}$, respectively in subarctic, midlatitude, and tropical climate types.

Figure 5 depicts the relationship between minimum altitude and AAV mass, taking into account various solar panel efficiencies ranging from $\eta_{\text{sc}} = 10\%$ to $\eta_{\text{sc}} = 40\%$. Our results indicate that as the mass of the AAV increases, the minimum altitude also increases. Furthermore, a notable observation is the inverse correlation between altitude and solar panel efficiency at a specific mass; higher efficiency corresponds to lower altitude requirements. For example, for $m = 60\,\text{kg}$, the corresponding minimum altitudes are $h_{\min} = 5.63\,\text{km}$, $h_{\min} = 7.1\,\text{km}$, $h_{\min} = 8.6\,\text{km}$, and $h_{\min} = 10\,\text{km}$, respectively, for solar panel efficiencies of $\eta_{\text{sc}} = 10\%$, $\eta_{\text{sc}} = 20\%$,$\eta_{\text{sc}} = 30\%$, and $\eta_{\text{sc}} = 40\%$.

In Figure 3, we observed variation of the optimized altitude across latitudes, spanning tropical to subarctic climates. Winter shows a consistent alignment between maximum and minimum altitudes. Spring exhibits a latitude-dependent decrease until subarctic regions, followed by a rise; fall and summer see consistent decreases with increasing latitude. In Figure 4, we further explored variation of optimized altitude throughout the year, showing an initial decrease with days until a specific point, followed by an ascent. Lower minimum altitudes suggest enhanced solar energy harvest efficiency, ensuring energy balance over the mission. Figure 6 presents a three-dimensional illustration showcasing minimum altitude in relation to both the day of the year and geographical location. Notably, both factors exert a substantial influence on the minimum altitude necessary for sustainable AAV operation. The graphical representation clearly shows that as latitude increases, the minimum altitude also rises. Additionally, as the day of the year approaches winter, there is a noticeable increase in the minimum altitude, aligning with the expectation of meeting the constraint specified in (14). This correlation underscores the significant impact of both geographical location and time of year on the required minimum altitude for effective AAV operation.

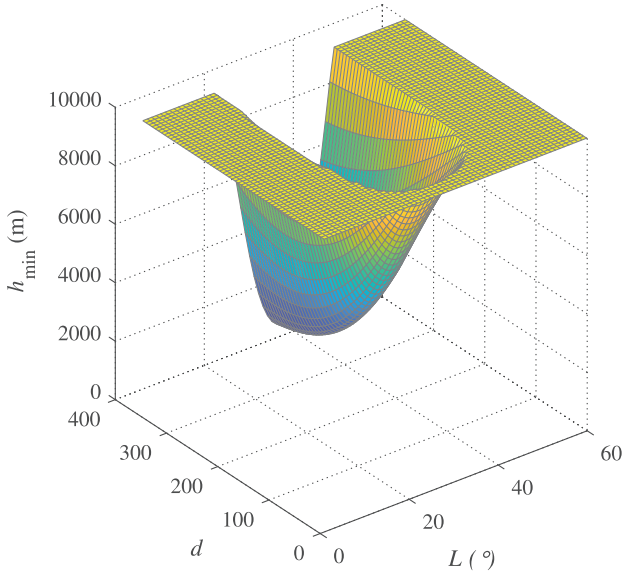

FIGURE 6. Minimum altitude with respect to latitude and day of the year.

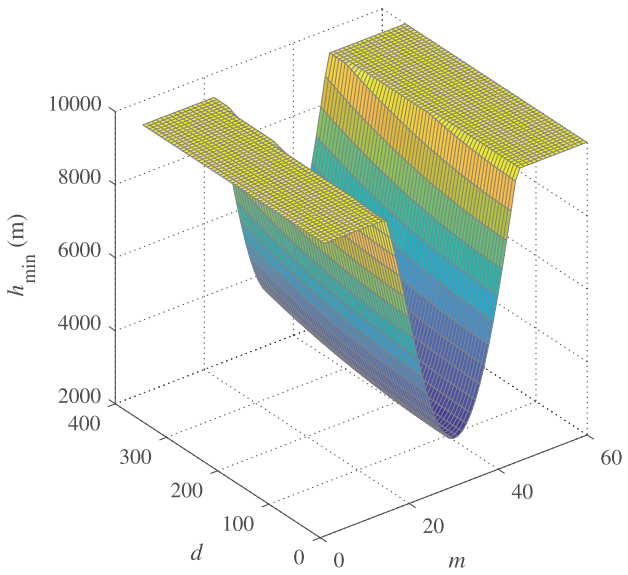

FIGURE 7. Minimum altitude with respect to day of the year and the mass of the AAV.

To have further insights into observations earlier made in Figure 4 and 5, Figure 7 provides a three-dimensional representation that illustrates minimum altitude in relation to both the day of the year and AAV mass. Notably, both factors exert a significant influence on the minimum altitude necessary for sustainable AAV operation. The visual depiction reveals a clear trend where an increase in the mass of the AAV corresponds to a higher minimum altitude. Additionally, as the day of the year approaches winter, there is a discernible rise in the minimum altitude, aligning with the objective of meeting the constraint specified in (14).

V. CONCLUSION

In this paper, we considered a solar-powered fixed-wing AAV designed to provide backhaul connectivity to base stations on the ground. We investigated the minimum operation altitude at which the AAV can sustain flight without depleting its battery. The significance of minimizing operational altitude lies in its critical role for sustainable and time-sensitive missions, ensuring rapid responses to emergencies and facilitating closer proximity for prompt AAV intervention. We derived a closed-form solution for this minimum altitude elucidating its dependence on various influential factors. Our study pointed out key parameters, including geographical location, day of the year, AAV mass, and solar panel efficiency, as critical determinants of this operational altitude.

REFERENCES

[1] M. M. Azari et al., "Evolution of non-terrestrial networks from 5G to 6G: A survey," *IEEE Commun. Surveys Tuts.*, vol. 24, no. 4, pp. 2633–2672, 4th Quart., 2022.

[2] M. Elamassie and M. Uysal, "Free space optical communication: An enabling backhaul technology for 6G non-terrestrial networks," *Photonics*, vol. 10, no. 11, p. 1210, 2023.

[3] M. Alzenad, M. Z. Shakir, H. Yanikomeroglu, and M.-S. Alouini, "FSO-based vertical backhaul/fronthaul framework for 5G+ wireless networks," *IEEE Commun. Mag.*, vol. 56, no. 1, pp. 218–224, Jan. 2018.

[4] H. S. Khallaf and M. Uysal, "Comprehensive study on UAV-based FSO links for high-speed train backhauling," *Appl. Opt.*, vol. 60, no. 27, pp. 8239–8247, 2021.

[5] M. T. Dabiri and S. M. S. Sadough, "Optimal placement of UAV-assisted free-space optical communication systems with DF relaying," *IEEE Commun. Lett.*, vol. 24, no. 1, pp. 155–158, Jan. 2020.

[6] M. T. Dabiri et al., "UAV-assisted free space optical communication system with amplify-and-forward relaying," *IEEE Trans. Veh. Technol.*, vol. 70, no. 9, pp. 8926–8936, Sep. 2021.

[7] M. K. Shehzad, A. Ahmad, S. A. Hassan, and H. Jung, "Backhaul-aware intelligent positioning of UAVs and association of terrestrial base stations for fronthaul connectivity," *IEEE Trans. Netw. Sci. Eng.*, vol. 8, no. 4, pp. 2742–2755, Oct.–Dec. 2021.

[8] M. T. Dabiri, M. Hasna, N. Zorba, T. Khattab, and K. A. Qaraqe, "Enabling long mmWave aerial backhaul links via fixed-wing UAVs: Performance and design," *IEEE Trans. Commun.*, vol. 71, no. 10, pp. 6146–6161, Oct. 2023.

[9] C. Qiu, Z. Wei, Z. Feng, and P. Zhang, "Backhaul-aware trajectory optimization of fixed-wing UAV-mounted base station for continuous available wireless service," *IEEE Access*, vol. 8, pp. 60940–60950, 2020.

[10] X. Zhang et al., "3D trajectory optimization for UAV-assisted hybrid FSO/RF network with moving obstacles," *IEEE Trans. Aerosp. Electron. Syst.*, early access, Sep. 18, 2024, doi: 10.1109/TAES.2024.3462685.

[11] J.-H. Lee, J. Park, M. Bennis, and Y.-C. Ko, "Integrating LEO satellites and multi-UAV reinforcement learning for hybrid FSO/RF non-terrestrial networks," *IEEE Trans. Veh. Technol.*, vol. 72, no. 3, pp. 3647–3662, Mar. 2023.

[12] T. V. Nguyen, H. D. Le, N. T. Dang, and A. T. Pham, "On the design of rate adaptation for relay-assisted satellite hybrid FSO/RF systems," *IEEE Photon. J.*, vol. 14, no. 1, pp. 1–11, Feb. 2022.

[13] L. Ag, "High altitude platform stations (HAPS)-a future key element of broadband infrastructure," HAPS Alliance, Wakefield, MA, USA, White Paper, 2015. [Online]. Available: https://www.leichtwerk.de/fileadmin/start/HAPS_WhitePaper_A11_e.pdf

[14] C. Sun, X. Xiong, Z. Zhai, W. Ni, T. Ohtsuki, and X. Wang, "Max–min fair 3D trajectory design and transmission scheduling for solar-powered fixed-wing UAV-assisted data collection," *IEEE Trans. Wireless Commun.*, vol. 22, no. 12, pp. 8650–8665, Dec. 2023.

[15] Y. Lun, P. Yao, and Y. Wang, "Trajectory optimization of SUAV for marine vessels communication relay mission," *IEEE Syst. J.*, vol. 14, no. 4, pp. 5014–5024, Dec. 2020.
[16] R.-R. Lu, Y. Ma, S. H. Lin, B. Zhang, Q. Wang, and J. Y. Wang, "Energy-efficient trajectory optimization for UAV-based hybrid FSO/RF communications with buffer constraints," *Entropy*, vol. 23, p. 1596, Nov. 2021.
[17] J.-S. Lee and K.-H. Yu, "Optimal path planning of solar-powered UAV using gravitational potential energy," *IEEE Trans. Aerosp. Electron. Syst.*, vol. 53, no. 3, pp. 1442–1451, Jun. 2017.
[18] S. C. Arum, D. Grace, P. D. Mitchell, M. D. Zakaria, and N. Morozs, "Energy management of solar-powered aircraft-based high altitude platform for wireless communications," *Electronics*, vol. 9, no. 1, p. 179, 2020.
[19] Z. Yang, W. Xu, and M. Shikh-Bahaei, "Energy efficient UAV communication with energy harvesting," *IEEE Trans. Veh. Technol.*, vol. 69, no. 2, pp. 1913–1927, Feb. 2020.
[20] P. Oettershagen et al., "Design of small hand-launched solar-powered UAVs: From concept study to a multi-day world endurance record flight," *J. Field Robot.*, vol. 34, no. 7, pp. 1352–1377, 2017. [Online]. Available: https://api.semanticscholar.org/CorpusID:41699173
[21] S. Wang, X. Qin, W. Xu, Z. Zhang, H. Li, and N. Ma, "Aerodynamic-aware energy saving for fixed-wing UAV under data collection requirements," in *Proc. IEEE Int. Conf. Commun. Workshops (ICC Workshops)*, 2021, pp. 1–6.
[22] F. B. Teixeira, R. Campos, and M. Ricardo, "Height optimization in aerial networks for enhanced broadband communications at sea," *IEEE Access*, vol. 8, pp. 28311–28323, 2020.
[23] K. Sekine, T. Tatsukawa, E. Itoh, and K. Fujii, "Multi-objective takeoff time optimization using cellular automaton-based simulator," *IEEE Access*, vol. 9, pp. 79461–79476, 2021.
[24] I. K. Singgih, J. Lee, and B.-I. Kim, "Node and edge drone surveillance problem with consideration of required observation quality and battery replacement," *IEEE Access*, vol. 8, pp. 44125–44139, 2020.
[25] Y. Sun et al., "OCO-2 advances photosynthesis observation from space via solar-induced chlorophyll fluorescence," *Science*, vol. 358, no. 6360, 2017, Art. no. eaam5747.
[26] J. Jessin, C. Heinzlef, N. Long, and D. Serre, "A systematic review of UAVs for island coastal environment and risk monitoring: Towards a resilience assessment," *Drones*, vol. 7, no. 3, p. 206, 2023.
[27] J. Miller and S. Uludag, "Energy-efficiency framework for fixed-wing UAV communications with variable altitude," in *Proc. IEEE Int. Conf. Commun. Workshops (ICC Workshops)*, 2021, pp. 1–6.
[28] Y. Zeng and R. Zhang, "Energy-efficient UAV communication with trajectory optimization," *IEEE Trans. Wireless Commun.*, vol. 16, no. 6, pp. 3747–3760, Jun. 2017.
[29] C. Peng, J. Wang, and D. Wu, "Impacts of air density fluctuations toward the mass measurements of a 1 kg silicon sphere," *IEEE Access*, vol. 8, pp. 140840–140847, 2020.
[30] N. C. A. Vishwath, P. Dhanwani, R. K. Baghel, R. Bendale, and P. Mehta, "Solar-powered fixed-wing UAV: Fabrication procedures with design methods," in *Recent Advances in Aerospace Engineering*, S. Singh, P. J. Ramulu, and S. S. Gautam, Eds. Singapore: Springer, 2024, pp. 65–83.
[31] Z. Li, Y. Yang, J. Jiao, and X. Ma, "An optimal energy absorption and utilization design for deformable/reconfigurable modular solar-powered UAVs in near space," *IEEE Access*, vol. 10, pp. 91948–91962, 2022.
[32] C. Zhang, C. Zhang, L. Li, and Q. Guo, "Parameter analysis of power system for solar-powered unmanned aerial vehicle," *Appl. Energy*, vol. 295, Aug. 2021, Art. no. 117031. [Online]. Available: https://www.sciencedirect.com/science/article/pii/S0306261921004931
[33] X.-Z. Gao, Z.-X. Hou, Z. Guo, R.-F. Fan, and X.-Q. Chen, "The equivalence of gravitational potential and rechargeable battery for high-altitude long-endurance solar-powered aircraft on energy storage," *Energy Convers. Manag.*, vol. 76, pp. 986–995, Dec. 2013. [Online]. Available: https://www.sciencedirect.com/science/article/pii/S0196890413004822
[34] D. Mitridis, S. Kapsalis, D. Terzis, and P. Panagiotou, "An evaluation of fixed-wing unmanned aerial vehicle trends and correlations with respect to NATO classification, region, EIS date and operational specifications," *Aerospace*, vol. 10, no. 4, p. 382, 2023. [Online]. Available: https://www.mdpi.com/2226-4310/10/4/382



KHADIJEH ALI MAHMOODI (Member, IEEE) recieved the M.Sc. degree in 2019, and the Ph.D. degree from Ozyegin University. She began her academic journey with the Optoelectronics and Optical Communications Research Laboratory Research Center, Isfahan University of Technology, Isfahan, Iran, in 2016. Seeking new challenges and opportunities, her passion for advancing communication technologies led her to join the Communication Theory and Technologies Research Group, Ozyegin University, Istanbul, Türkiye, in 2020, where she embarked on a Ph.D. journey under the mentorship of Prof. M. Uysal. She is currently a Postdoctoral Researcher of High-Speed Communications with ESYCOM Laboratory, Paris, France. During her Ph.D., she was actively involved in the prestigious ENLIGHTEM Project, where she served as a Marie Curie Early-Stage Researcher. This remarkable opportunity allowed her to collaborate with leading experts and researchers, broadening her perspective and fostering international collaboration. The project has since been completed. Her research interests encompass a diverse range of topics within the realm of communication networks. She is particularly fascinated by nonterrestrial networks, specifically focusing on their energy efficiency and improving them. Additionally, her interests include low-energy visible light communication systems, underwater sensor networks, energy harvesting techniques, and the optimization of trajectories for AUVs and AAVs in communication networks.



MOHAMMED ELAMASSIE (Senior Member, IEEE) received the Ph.D. degree in electrical and electronics engineering from Ozyegin University, Istanbul, Türkiye, in 2020.

He currently serves as an Assistant Professor with Ozyegin University, where he serves as an Executive Co-Director of both the Center of Excellence in Optical Wireless Communication Technologies and the Communication Theory and Technologies Research Group. He has authored over 70 publications in reputable journals and conferences, with 1400+ Google Scholar Citations and an H-index of 20. His research interests lie in the broad area of wireless communications. Specific topics include HAPS/AAV-based optical wireless communication, atmospheric attenuation models for visible and infrared wavelengths, free space optical communication, optical turbulence, visible light communications (indoor, outdoor, and underwater), performance analysis over fading channels and time-varying channels, channel estimation and equalization, and channel modeling.

Dr. Elamassie's major distinctions include the Best Paper Award at the IEEE International Black Sea Conference on Communications and Networking in 2019. He is also the recipient of the 2020 IEEE Turkey Doctoral Dissertation Award. Actively engaged in the academic community, He has several editorial positions, including serving as an Editor for the IEEE TRANSACTIONS ON COMMUNICATIONS since April 2024, an Associate Editor for FRONTIERS IN MARINE SCIENCE since May 2023, and as a Review Editor on the editorial boards of FRONTIERS IN COMMUNICATIONS AND NETWORKS' specialty sections 'Non-Conventional Communications and Networks' and 'Wireless Communications.' Additionally, he has served as a Guest Editor for a Special Issue at *Photonics* (MDPI). Lastly, he has recently joined the editorial board of the journal *Comm&Optics Connect* as a Regional Editor for the Middle East. He is a Senior Member of Optica, and serves as an Optica Traveling Lecturer.



MURAT UYSAL (Fellow, IEEE) received the B.Sc. and M.Sc. degrees in electronics and communication engineering from Istanbul Technical University, Türkiye, in 1995 and 1998, respectively, and the Ph.D. degree in electrical engineering from Texas A&M University at College Station, College Station, USA, in 2001.

He began his academic career as an Assistant Professor with the University of Waterloo, Canada, in 2002, and was promoted to an Associate Professor with tenure in 2007. In 2011, he joined Ozyegin University, Turkey, where he served as the Department Chair of Electrical and Electronics Engineering and the Founding Director of Center of Excellence, Optical Wireless Communication Technologies. Since 2023, he has been with New York University Abu Dhabi as a Professor of Electrical Engineering. His research interests are in the broad area of communication theory with a particular emphasis on the physical layer aspects of wireless communication systems in radio and optical frequency bands. On these topics, he has authored some 400 journal and conference papers and received more than 22k citations with an H-index of 66.

Dr. Uysal's major distinctions include the NSERC Discovery Accelerator Award in 2008, the University of Waterloo Engineering Research Excellence Award in 2010, the Turkish Academy of Sciences Distinguished Young Scientist Award in 2011, the Ozyegin University Outstanding Researcher Award in 2014, the National Instruments Engineering Impact Award in 2017, the Elginkan Foundation Technology Award in 2018, the IEEE Communications Society Best Survey Paper Award in 2019, the IEEE Turkey Section Outstanding Service Award in 2021, and the Mustafa Prize and Tubitak Science Award in 2023. He currently serves as an Area Editor for IEEE TRANSACTIONS ON COMMUNICATIONS. In the past, he served as an Editor for IEEE TRANSACTIONS ON COMMUNICATIONS, IEEE TRANSACTIONS ON WIRELESS COMMUNICATIONS, IEEE TRANSACTIONS ON VEHICULAR TECHNOLOGY, and IEEE COMMUNICATIONS LETTERS. He was involved in the organization of several IEEE conferences at various levels. In particular, he served as the Technical Program Committee Chair of major IEEE conferences, including WCNC 2014, PIMRC 2019, and VTC-Fall 2019. From 2011 to 2015, he was the Chair of EU COST Action OPTICWISE, a high-profile consolidated European scientific platform which brought together more than 150 researchers in the research area of optical wireless communication. He is the former Chair of IEEE Turkey Section.